J. Cent. South Univ. (2021) 28: 1955−1965
DOI: https://doi.org/10.1007/s11771-021-4744-4

Springer

Microwave hydrothermal synthesis, characterization and excellent uranium adsorption properties of $CoFe_2O_4$@rGO nanocomposite

WU Shui-sheng(伍水生)[1], LAN Dong-hui(兰东辉)[1], ZHANG Xiao-wen(张晓文)[2], HUANG Yi(黄毅)[3], DENG Xing-hong(邓兴红)[1], AU Chak-tong(区泽棠)[1], YI Bing(易兵)[1]

1. Hunan Provincial Key Laboratory of Environmental Catalysis & Waste Recycling, School of Materials and Chemical Engineering, Hunan Institute of Engineering, Xiangtan 411104, China;
2. School of Resource & Environmental and Safety Engineering, University of South China, Hengyang 421001, China;
3. School of Management, Hunan Institute of Engineering, Xiangtan 411104, China

Abstract: To improve the adsorption performance and simplify uranium separation from aqueous media in post-treatment processes, a magnetic $CoFe_2O_4$@rGO composite was synthesized by microwave-hydrothermal method. The results of XRD, Raman, TEM/HRTEM, FTIR, BET and VSM characterization show that spinel-type cobalt ferrite $CoFe_2O_4$ nanoparticles ca. 13.4 nm in size are dispersedly anchored on the graphene sheet, and the saturation magnetization of the nanocomposite is 46.7 mA/(m^2·g). The effects of different pH, initial concentration and other conditions on uranium adsorption capacity were investigated, and adsorption kinetics equations were fitted to determine the adsorption behaviour of uranium on $CoFe_2O_4$@rGO in simulated uranium-containing seawater. It was observed that the uranium adsorption capacity of $CoFe_2O_4$@rGO composite at pH=5 is 127.6 mg/g, which is 1.31 and 2.43 times that of rGO and pure $CoFe_2O_4$. The adsorption process conforms to Langmuir and quasi-second-order kinetic model. The excellent adsorption performance of $CoFe_2O_4$@rGO makes it potentially useful in the treatment of uranium-polluted water.

Key words: $CoFe_2O_4$; graphene; uranium; adsorption properties

Cite this article as: WU Shui-sheng, LAN Dong-hui, ZHANG Xiao-wen, HUANG Yi, DENG Xing-hong, AU Chak-tong, YI Bing. Microwave hydrothermal synthesis, characterization and excellent uranium adsorption properties of $CoFe_2O_4$@rGO nanocomposite [J]. Journal of Central South University, 2021, 28(7): 1955−1965. DOI: https://doi.org/10.1007/s11771-021-4744-4.

1 Introduction

As an important strategic nuclide, uranium plays a pivotal role in nuclear applications. With the development of nuclear-related technologies, there is a large amount of radioactive wastewater due to uranium contamination. It is hence of great significance to develop environment-benign methods that are low cost and highly efficient for the adsorption and separation of uranium. The current approaches for treating uranium-containing wastewater include flocculation [1], biological reduction and precipitation [2], reverse osmosis [3], ion exchange [4] and adsorption method [5, 6]. Among the above methods, adsorption has the

Foundation item: Project(19B126) supported by the Scientific Research Fund of Hunan Provincial Education Department, China; Project(21772035) supported by the National Natural Science Foundation of China; Projects(2018JJ3099, 2019JJ40058) supported by the Provincial Natural Science Foundation of Hunan, China; Project supported by the Innovation and Entrepreneurship Training Program of Hunan Institute of Engineering, China
Received date: 2020-05-09; **Accepted date:** 2020-12-01
Corresponding author: YI Bing, PhD, Professor; Tel: +86-13203218660; E-mail: bingyi2004@126.com; ORCID: https://orcid.org/0000-0002-8513-7051

advantages of low cost, easy operation, no need for large equipment, high uranium removal rate, and no secondary pollution. It is known that the type and morphology of adsorbents have a significant effect on adsorption efficiency. Adsorbents such as clay minerals [7], hydrotalcite [8, 9], metal oxides [10], resin [11] and MOF [6] have long been used for the treatment of uranium in water media worldwide. Nonetheless, shortcomings such as high preparation cost and/or low adsorption efficiency limit the use of these adsorbents, and there is still an urgent need for the development of practical materials for uranium adsorption.

With ultra-high surface area, rich functional groups, and good chemical stability, graphene has high potential in wastewater treatment [9]. However, due to strong van der Waals interaction, there is severe agglomeration of graphene in water, resulting in the loss of effective surface area, and hence reduction of adsorption capacity [10]. Furthermore, because it is not easy to separate graphene from the water phase, there could be secondary pollution. In recent years, magnetic ferrite spinel-graphene composites were used as effective adsorbents that can be rapidly separated by an external magnetic field [11, 12]. In addition, the magnetic nanoparticles can help prevent the aggregation of graphene layers, leading to improved adsorption performance. For example, WU et al [13] prepared magnetic polysaccharide/graphene oxide@Fe_3O_4 gel beads for efficient adsorption of heavy metal ions such as Cu^{2+}, Cd^{2+} and Pb^{2+} from wastewater; ZHAO et al [14] prepared magnetic Fe_3O_4/graphene composites for effective uranium scavenging. BAI et al [15] studied the effects of reduced graphene oxide (rGO) content on the adsorption of rhodamine B and other dyes over composites comprised of rGO and manganese ferrite. Despite numerous magnetic composites were successfully used as adsorbents for the removal of pollutants in water systems, the application of them is limited due to factors such as complicated preparation, low adsorption capacity, poor separation efficiency, and harsh pH requirement. Endowed with unique properties, $CoFe_2O_4$@rGO composites have been widely used in catalysis, electromagnetic absorption, and lithium-ion batteries [16−18]. However, to the best of our awareness, there have been no reports on the synthesis of $CoFe_2O_4$@rGO composites using microwave hydrothermal method, as well as their use as adsorbents for the removal of uranium or other radioactive elements.

There are methods for the synthesis of nanomaterials including those that are based on hydrothermal, chemical precipitation, sol-gel, and ultrasonic approaches [19]. Most of these methods, however, have shortcomings such as easy aggregation of nanoparticles and long reaction time. In this paper, we reported the use of a microwave hydrothermal method for the synthesis of $CoFe_2O_4$@rGO. Compared to traditional hydrothermal synthesis, the deployment of microwave hydrothermal has additional advantages such as low energy consumption, rapid grain formation, and uniform particle size [20]. The morphology and structure of the magnetic $CoFe_2O_4$@rGO composite were characterized by XRD, Raman, FTIR, TEM, BET and VSM techniques. The adsorption of uranyl ions on $CoFe_2O_4$@rGO was studied, and the effect of experimental conditions such as time and pH on the adsorption was discussed. The excellent performance of $CoFe_2O_4$@rGO for uranium adsorption makes it potentially useful for the treatment of water that is contaminated with uranyl ions.

2 Experimental

2.1 Materials

Natural graphite (Alfar Aesar), uranium standard solution (100 μg/mL, Beijing Institute of Chemical Industry and Metallurgy), potassium permanganate ($KMnO_4$), iron (III) chloride hexahydrate ($FeCl_3·6H_2O$), cobalt chloride hexahydrate ($CoCl_2·6H_2O$), sulfuric acid (H_2SO_4, 98%), hydrogen peroxide (H_2O_2, 30%), ammonia ($NH_3·H_2O$, 25%) and other chemicals were of analytical grade.

2.2 Preparation and characterization of $CoFe_2O_4$@rGO

Graphene oxide (GO) was prepared by a modified Hummers method [21]. The $CoFe_2O_4$@rGO nanocomposite was synthesized using a microwave-employed hydrothermal method. First 0.01 g of GO was dispersed in 10 mL of deionized water, and the mixture was ultrasonically treated for 2 h. Then 30 mL of $FeCl_3$ and $CoCl_2$ aqueous solution of specific concentration were slowly added to the GO solution at room temperature under N_2 atmosphere. The pH of the reaction

solution was adjusted to 10 using a 30% ammonia solution. The total volume of the solution was controlled at ca. 60 mL and stirring was continued for 30 min. The obtained precursor mixture was transferred to a polytetrafluoroethylene reactor with an effective volume of 100 mL, and placed in an MDS-6 microwave hydrothermal synthesizer. The heating rate was 10 °C/min, and the reaction was held at 160 °C for 30 min. After reaction, the mixture was naturally cooled to room temperature. The dark black solution was filtrated and the collected powder was washed with deionized water and ethanol for three times, and dried in an oven at 50 °C for 12 h to obtain a black powder sample, which is herein denoted as $CoFe_2O_4$@rGO. Pure $CoFe_2O_4$ and rGO were also synthesized following the procedures; for the former, there was no addition of GO whereas for the latter no addition of $FeCl_3$ and $CoCl_2$ aqueous solutions.

2.3 Characterization

The phase structure and purity of GO, rGO, $CoFe_2O_4$, and $CoFe_2O_4$@rGO samples were analyzed by D8 Advance X-ray powder diffractometer (XRD, Bruker D8, radiation source Cu K$_\alpha$, wavelength 0.15406 nm, step size 0.04°, scanning range 20°−70°). The morphology of $CoFe_2O_4$@rGO was studied by TEM(H–7650B, 80 kV) and HRTEM (JEM-2010F, 120 kV). FTIR were carried out by Nicolet 6700 Fourier transform infrared spectrometer. Raman spectrum was analyzed by Raman spectrometer (Renishaw RM–1000, 514 nm, Ar-ion laser). Magnetic properties of synthetic samples were recorded on PPMS-9T at 298 K.

2.4 Adsorption experiment

40 mL of uranium solution of a particular concentration (10−100 mg/L) was added to an erlenmeyer flask, and the pH was adjusted to set value with 0.1 mol/L HCl or NaOH solution. After the addition of 8−60 mg of adsorbent into the flask, adsorption occurred with constant shaking at 298 K for a set time. After the adsorption process completed, the adsorbent was magnetically separated and the content of uranyl ions in the supernatant was analyzed by a MUA-type trace uranium measuring instrument. The adsorption capacity was calculated according to Eq. (1). The quasi-first-order kinetic and quasi-second-order kinetic models were used to evaluate the kinetic mechanism of the adsorption process, as shown in Eqs. (2) and (3), respectively [22]. As for the Langmuir and Freundlich isothermal adsorption equations, they are Eqs. (4) and (5) [23].

$$Q_e = \frac{(c_0 - c_e)V}{W} \tag{1}$$

$$\ln(Q_e - Q_t) = \ln Q_e - k_1 t \tag{2}$$

$$\frac{t}{Q_t} = \frac{1}{k_2 Q_e^2} + \frac{t}{Q_e} \tag{3}$$

$$Q_e = \frac{Q_m \cdot K_L \cdot c_e}{1 + K_L \cdot c_e} \tag{4}$$

$$Q_e = K_F \cdot c_e^n \tag{5}$$

where c_0 and c_e are the initial and adsorption equilibrium concentrations of uranium, respectively; W is the amount of adsorbent; V is the volume of the solution; Q_e and Q_t are the adsorption amounts at equilibrium and time t, respectively; k_1 is the Lagergren rate constant; k_2 is quasi-second-order kinetic adsorption rate constant; K_L and K_F are the Langmuir and Freundlich constants; n is the Freundlich adsorption index.

3 Results and discussion

3.1 Material characterization

Figure 1 shows the XRD patterns of GO, rGO and $CoFe_2O_4$@rGO. In the GO pattern, the diffraction peak at 10.8° is characteristic of graphite oxide. After microwave hydrothermal treatment, the peak at 10.8° has completely disappeared, and a weak broad peak at 24.5° attributable to reduced graphene oxide (002) appeared [24]. The XRD pattern of $CoFe_2O_4$@rGO shows a weak rGO peak at

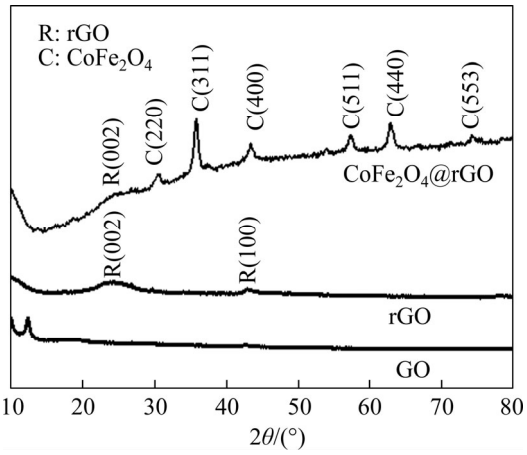

Figure 1 XRD patterns of GO, rGO and $CoFe_2O_4$@rGO

24.6°, and other peaks at 30.2, 35.6, 43.2, 57.1, 62.6 and 74.5° appear which can be indexed to the (220), (311), (400), (511), (440) and (533) crystal planes of spinel-type $CoFe_2O_4$, respectively (JCPDS PDF card 22-1086) [25]. The average particle size of $CoFe_2O_4$ nanoparticles in the composite calculated using the Debye-Scherrer equation is about 14.0 nm. The XRD results indicate successful synthesis of the $CoFe_2O_4$@rGO complex.

The FTIR spectra of GO and $CoFe_2O_4$@rGO are shown in Figure 2(a). According to literature, the infrared characteristic peaks of GO at 3416 and 1725 cm^{-1} are due to the stretching vibration of O—H and C═O, those at 1622, 1387, 1227 cm^{-1} are due to the stretching vibration of C—C, H_2O, and O═C—O, while that at 1061 cm^{-1} is due to the stretching vibration of C—O—C [26]. Compared with GO, there is near complete disappearance of the characteristic peaks of oxygen-containing functional groups such as O—H, C═O, and C—O—C in the $CoFe_2O_4$@rGO case, implying that GO has been reduced to rGO. In addition, the strong absorption peak at 590 cm^{-1} is the vibrational peak of Fe—O, indicating successful loading of $CoFe_2O_4$ on rGO. Figure 2(b) shows the Raman spectra of GO and $CoFe_2O_4$@rGO, the G band at 1588 cm^{-1} is ascribed to the vibration of sp^2 carbon atom, while the D band at 1346 cm^{-1} to the vibration of defects and disordered sp^3 carbon atoms of graphene materials [27]. The D-band to G-band intensity ratio (I_D/I_G) of $CoFe_2O_4$@rGO (1.072) is higher than that of GO (0.931). It is possible that the reduction of GO and anchoring of $CoFe_2O_4$ nanoparticles on rGO cause an increase of disordered carbon atoms on the graphene surface [28].

The morphology of nanomaterials can be visually observed using the TEM and HRTEM techniques. Figure 3(a) shows the gauze-like morphology of GO curvy sheet. In Figure 3(b), one can see the clustering of $CoFe_2O_4$ nanoparticles which are 20−30 nm in size. Figures 3(c) and (d) are the TEM images of $CoFe_2O_4$@rGO with different magnifications, showing the $CoFe_2O_4$ nanoparticles are uniformly distributed on the graphene sheet (Figure 3(c)). The TEM image of higher magnification shows that the particle size of $CoFe_2O_4$ nanoparticles is about 13.4 nm (Figure 3(e)), which is consistent with the XRD result. The HRTEM image of $CoFe_2O_4$@rGO shows lattice fringes of 0.293 nm in spacing (Figure 3(f)), matching the (220) interplanar spacing of spinel-structure $CoFe_2O_4$ [29].

Figure 4(a) shows the magnetization hysteresis loops of $CoFe_2O_4$ and $CoFe_2O_4$@rGO collected at room-temperature. The $CoFe_2O_4$ nanoparticles and the $CoFe_2O_4$@rGO nanocomposite display superparamagnetism with coercivity close to zero. The saturation magnetizations of $CoFe_2O_4$ and $CoFe_2O_4$@rGO composite are 65.6 and 46.7 mA/(m^2·g), respectively. The $CoFe_2O_4$@rGO composite has weaker magnetic properties than $CoFe_2O_4$, plausibly due to the coating of non-magnetic graphene on the surface of magnetic $CoFe_2O_4$. The $CoFe_2O_4$@rGO nanocomposite with a concentration of 2 mg/mL can be quickly separated from water under the action of an external magnetic field (inset of Figure 4(b)). Figure 5(b) shows the N_2 adsorption−desorption and pore size distribution curves of $CoFe_2O_4$@rGO. The nanocomposite exhibits type-IV isotherm, and a H2-type hysteresis loop appears in the P/P^* relative pressure range of 0.65−0.95, which indicate existence of mesoporous

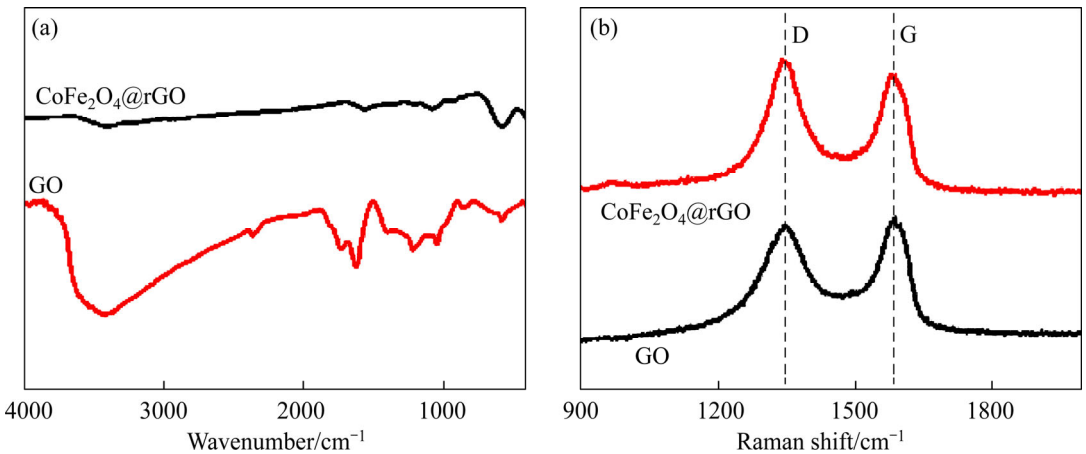

Figure 2 FTIR spectra (a) and Raman spectra (b) of GO and $CoFe_2O_4$@rGO

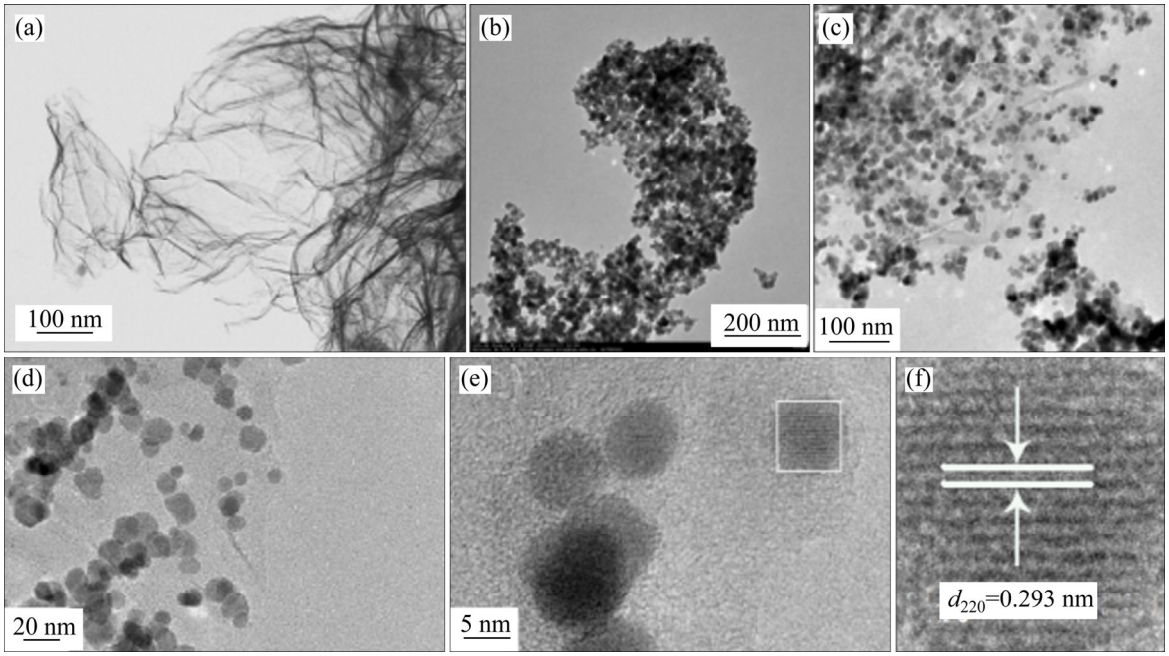

Figure 3 TEM images of (a) GO, (b) $CoFe_2O_4$, (c, d) $CoFe_2O_4$@rGO; (e)TEM and (f) HRTEM image of $CoFe_2O_4$@rGO

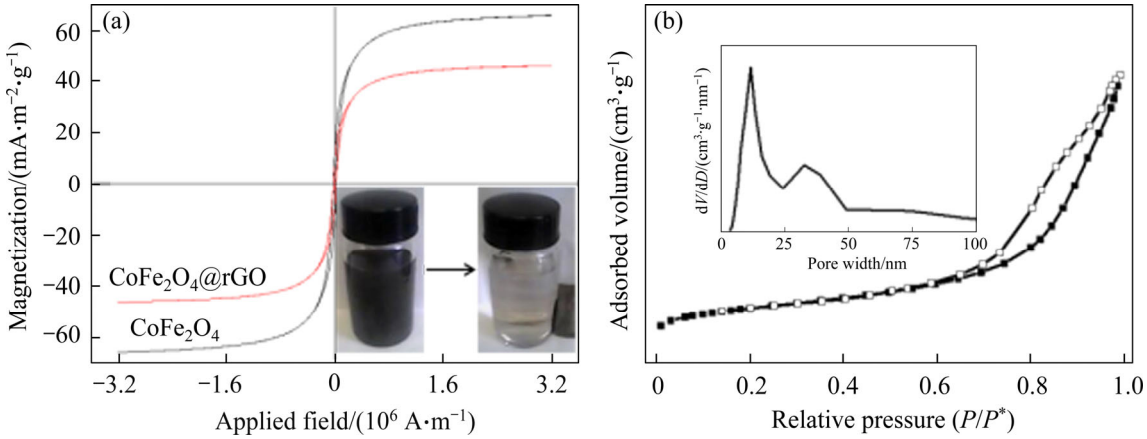

Figure 4 Magnetization curves (inset are pictures illustrating $CoFe_2O_4$@rGO magnetic separation) (a) and nitrogen adsorption–desorption isotherm curves of $CoFe_2O_4$@rGO (b)

structure. The specific surface area and pore volume of $CoFe_2O_4$@rGO are 119.76 m^2/g and 0.1822 cm^3/g, respectively. The distribution of pore size is mainly at 4.76 nm as calculated by BJH model (inset of Figure 5(b)). The large specific surface area of $CoFe_2O_4$@rGO indicates high adsorption capacity and abundant adsorption sites, thereby facilitating effective adsorption.

3.2 Adsorption performance

The effects of solution pH (2−11) on the removal of uranium (initial concentration 100 mg/L) using $CoFe_2O_4$, rGO and $CoFe_2O_4$@rGO are illustrated in Figure 5. It can be seen that rGO exhibits the lowest adsorption performance whereas

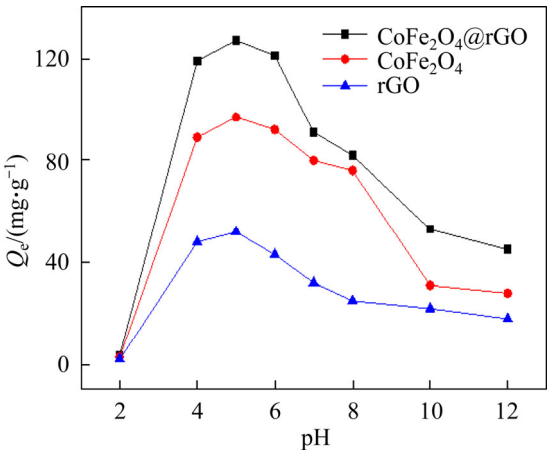

Figure 5 Influence of pH value on adsorption efficiency of as-synthesized materials (m/V=0.5 g/L, shaking time: 180 min)

$CoFe_2O_4$@rGO shows the highest. The $CoFe_2O_4$@rGO composite has a uranium adsorption capacity of 127.6 mg/g, which is 1.31 and 2.43 times that of rGO and pure $CoFe_2O_4$, respectively. The capacity of $CoFe_2O_4$@rGO for uranium adsorption is greatly affected by the pH value of the solution. When pH increases from 2.0 to 4.0, there is gradual increase of adsorption capacity. Within the pH range of 4.0−6.0, the adsorption capacity remains roughly unchanged. When pH is above 6.0, the adsorption capacity progressively decreases. It is considered that at pH<4, U(VI) exists as UO_2^{2+} in the solution, and the lower uranium adsorption capacity is due to the competition between H^+ and UO_2^{2+} for adsorption sites [27]. When pH is between 4 and 6, $(UO_2)_3(OH)_5^+$ dominates [30], and adsorption is significantly improved due to electrostatic interaction between positively charged $UO_2)_3(OH)_5^+$ and negatively charged $CoFe_2O_4$@rGO surface. When pH is larger than 8.0, $UO_2(CO_3)_2^{2-}$ and $UO_2(CO_3)_3^{4-}$ are the main uranium species, and these anions have low affinity with negatively charged $CoFe_2O_4$@rGO composite, leading to rapid decrease of adsorption capacity. The results show that the optimal pH for uranium adsorption on $CoFe_2O_4$@rGO is 5.0.

The effects of solid-liquid ratio and initial uranium concentration on the adsorption performance were further analyzed. The results of solid-liquid ratio are shown in Figure 6(a) (initial uranium concentration=40 mg/L), with the increase of solid-liquid ratio from 0.2 to 0.5 g/L, the uranium adsorption rate increases from 58.4% to 92.2%. When the solid-liquid ratio is further increased to 1.0 g/L, the uranium adsorption rate remains almost unchanged, but adsorption capacity continues to decrease. The possible reason is that all kinds of energy adsorption sites on $CoFe_2O_4$@rGO surface can be completely exposed for adsorption at low solid-liquid ratio, and the surface saturation is faster, so it shows higher adsorption capacity. However, at high solid-liquid ratio, most of the sites with lower energy are preferentially used for adsorption, resulting in the decrease of binding properties of the higher energy sites. In addition, the higher solid-liquid ratio will increase the probability of collision between adsorbent particles, thus resulting in aggregation. Both of them will reduce the adsorption capacity. Figure 6(b) shows the effect of initial uranium concentration on adsorption performance (solid-liquid ratio=0.5 g/L). With the increase or decrease of initial concentration, the adsorption capacity increases and the adsorption rate decreases. Therefore, the optimum solid-liquid ratio and initial are 0.5 g/L and 100 mg/L, respectively.

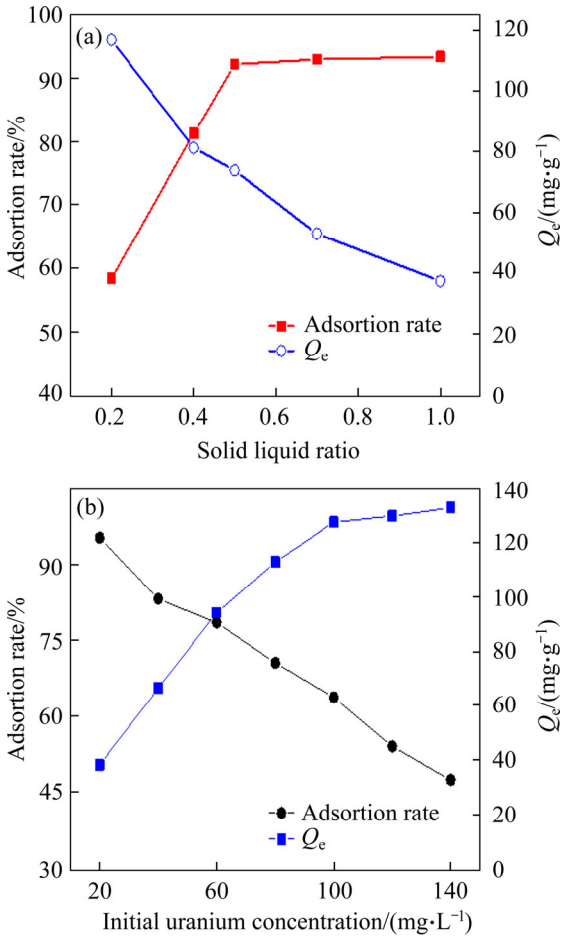

Figure 6 Effect of solid-liquid ratio (a) and initial uranium concentration (b) on adsorption efficiency (pH=5, shaking time: 180 min)

Adsorption kinetics of an adsorption process can reflect the adsorption efficiency of an adsorbent. The effect of adsorption time on uranium adsorption over $CoFe_2O_4$@rGO is depicted in Figure 7(a). It can be seen that there is rapid adsorption during the first 90 min, and then adsorption rate slows down before reaching equilibrium at 150 min. Therefore, to ensure adsorption equilibrium, the adsorption time was set to 150 min in subsequent experiments. The results show that the maximum adsorption capacity of $CoFe_2O_4$@rGO is 135.4 mg/g.

The quasi-first-order kinetic equation and quasi-second-order kinetic equation were fitted to the experimental data of uranium adsorption on $CoFe_2O_4$@rGO at 298 K. The results are shown in

Figures 7(b) and (c) and the related kinetic data are listed in Table 1. It is observed that the theoretical adsorption capacity calculated using the quasi-first-order kinetic model is inconsistent with the experimental data, and the correlation coefficient is relatively low (0.954), indicating that the adsorption of uranium by $CoFe_2O_4$@rGO does not conform to the quasi-first-order kinetic model. The theoretical saturated adsorption Q_e (cal) calculated according to the quasi-second-order kinetic equation is more in line with the experimental Q_e (exp), and the correlation coefficient is close to 1. Therefore, the adsorption process of uranium on $CoFe_2O_4$@rGO is better described by the quasi-second-order kinetic model.

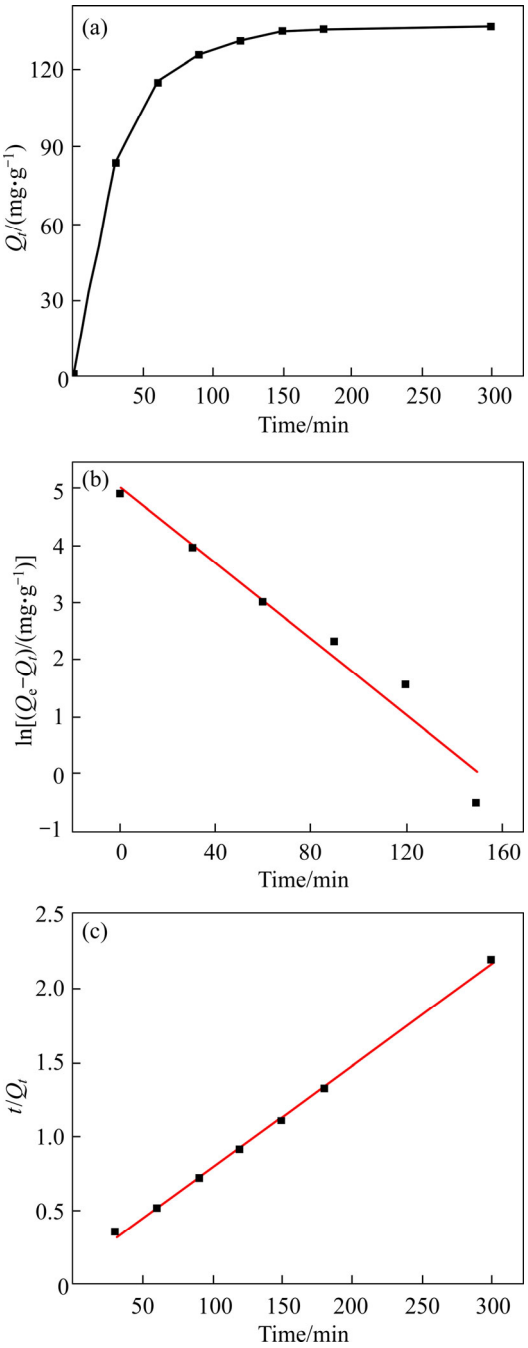

Figure 7 Uranium sorption of $CoFe_2O_4$@rGO versus time (a); pseudo-first-order (b) and pseudo-second-order adsorption fit plot (c) for uranium sorption (pH=5, m/V=0.5 g/L)

To further study the adsorption process, Langmuir and Freundlich isothermal adsorption models were used to analyze the adsorption equilibrium data. The results are shown in Figure 8 and the adsorption parameters are compiled in Table 2. The correlation coefficient (R^2) of Langmuir isotherm fitting for rGO and $CoFe_2O_4$@rGO is 0.998 and 0.998, respectively, which is higher than that of Freundlich isotherm fitting (0.848 and 0.798). It is clear that the adsorption processes of uranyl ions are more consistent with the Langmuir model, indicating uniform monolayer adsorption of uranyl ions on rGO and $CoFe_2O_4$@rGO. According to Langmuir adsorption isotherm calculation, the maximum capacity (Q_m) of $CoFe_2O_4$@rGO for uranium sorption at 25 °C is 160.5 mg/g. The fitting result of Freundrich isothermal adsorption model suggests that the n value is less than 1, and when $0<n<1$, it implies easy adsorption. This shows that $CoFe_2O_4$@rGO has a strong adsorption capacity for uranyl ions.

There are many kinds of metal ions in the actual uranium-containing wastewater, and these ions could affect the uranium adsorption performance of $CoFe_2O_4$@rGO, because they compete with uranyl ions for adsorption sites and obstruct the adsorption of uranium. Figure 9(a) shows the adsorption results of $CoFe_2O_4$@rGO in actual uranium-containing wastewater (initial pH value 4−6, c_{Na}: 0.3−10.0 mg/L, c_K: 0.3−10.0 mg/L, c_{Si}≤2.5 mg/L, c_{Ca}≤5.00 mg/L, c_{Fe}≤0.34 mg/L, c_{Mg}≤1.38 mg/L and a small amount of Al, B, Be, Cu, Mo, Ni, etc.). It can be seen that the adsorption capacity of $CoFe_2O_4$@rGO in uranium-containing seawater is

Table 1 Pseudo-first-order and pseudo-second-order model parameters for $CoFe_2O_4$@rGO

Kinetic model	T/°C	c/(mg·L^{-1})	Q_e (exp)/(mg·g^{-1})	Q_e (cal)/(mg·g^{-1})	k_1/(g·mg^{-1}·min^{-1})	k_2/(g·mg^{-1}·min^{-1})	R^2
Pseudo-first-order	25	100	128.4	4.65	0.0333		0.954
Pseudo-second-order	25	100	128.4	130.9		5.9×10^{-4}	0.997

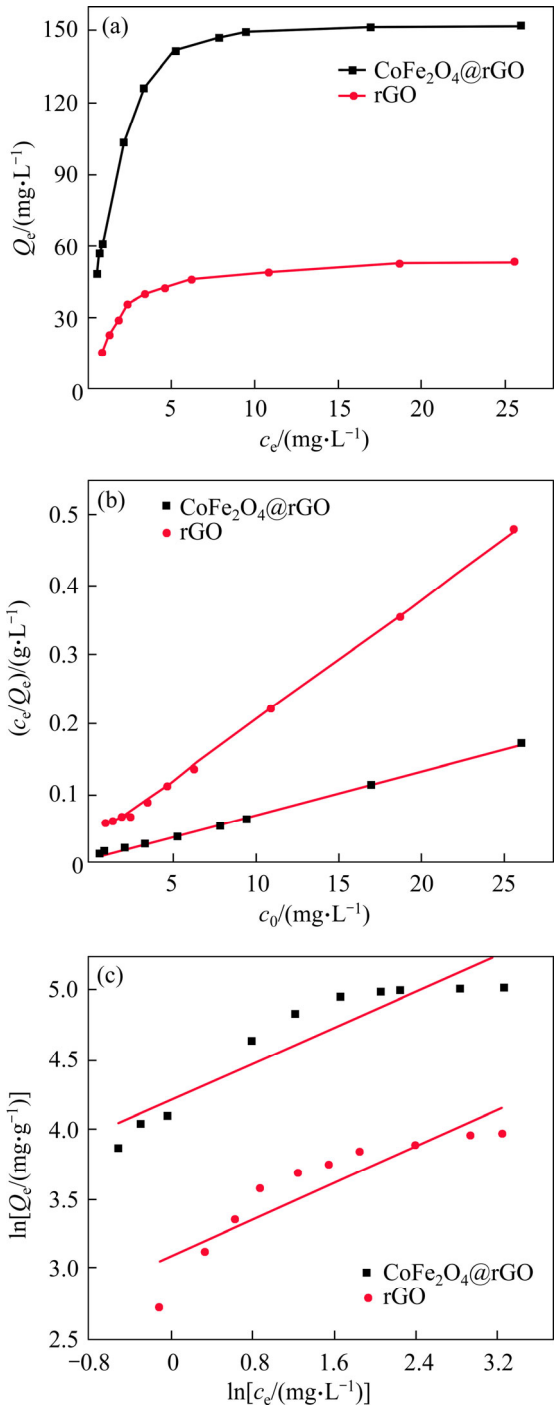

Figure 8 Adsorption isotherm (a), Langmuir model (b), and Freundlich model (c) of $CoFe_2O_4$@rGO and rGO

lower than that in a solution just with the presence of uranium. This may be due to the competitive adsorption of other metal ions and/or the pH of the uranium-containing seawater solution which is deviated from the optimal pH for uranium adsorption. The effect of the coexisting of Na^+, K^+, Ca^{2+} or Mg^{2+} cations on uranium adsorption performance was also investigated. The results show the co-presence of any of the four cations has little effect on the uranium adsorption performance of $CoFe_2O_4$@rGO (Figure 9(b)). Among them, Na^+ and K^+ have insignificant effect on the uranium adsorption performance of $CoFe_2O_4$@rGO. The effect of Ca^{2+} and Mg^{2+} of higher valence is marginally more significant. The above results indicate that $CoFe_2O_4$@rGO has good selectivity towards uranium ions.

The recycling of the adsorbent is an important indicator of its practical application value. The adsorption−desorption cycle experiments of uranyl solution by $CoFe_2O_4$@rGO nanocomposite was carried out. In the desorption experiment, the adsorbent after the end of the adsorption was stirred with a desorption solution of 0.1 mol/L of NaOH, $NaHCO_3$ or Na_2CO_3 for 60 min, and the regenerated adsorbent was obtained by drying after applying magnetic separation. Figure 10(a) shows that the desorption rates of uranyl ion desorbed from the adsorbent were 61.2%, 92.3% and 84.5%, indicating that the desorption effect is the best when using $NaHCO_3$ desorption solution and used in subsequent adsorption−desorption cycle experiments. Figure 10(b) shows that after five adsorption−desorption cycles, the adsorption capacity was slightly reduced from 126 to 108.5 mg/g, and still reached about 98% of the first adsorption capacity. It can be seen that $CoFe_2O_4$@rGO has better cycle performance and has potential for practical applications.

4 Conclusions

Magnetic $CoFe_2O_4$@rGO composite was successfully prepared using microwave hydrothermal method. The structure and

Table 2 Adsorption parameters for Langmuir and Freundlich isotherm models

Adsorbent	Langmuir model parameter			Freundlich model parameter		
	Q_m/(mg·g^{-1})	k_L/(L·mg^{-1})	R^2	n	k_F(mg^{1-n}·L^n·mg^{-1})	R^2
rGO	57.5	0.54	0.998	0.3275	21.98	0.848
$CoFe_2O_4$@rGO	160.5	0.89	0.998	0.3316	67.36	0.798

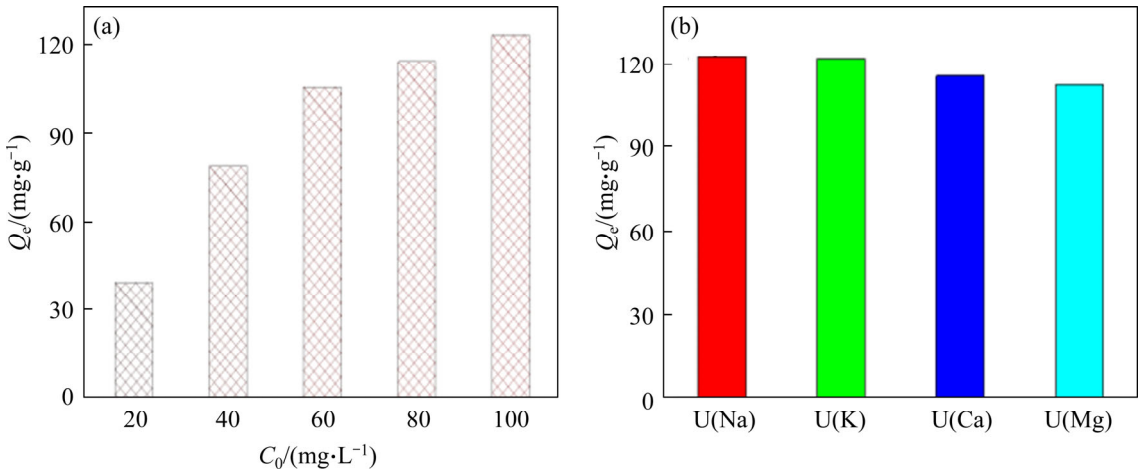

Figure 9 Uranium adsorption on $CoFe_2O_4$@rGO in actual wastewater (a) and effect of coexisting ions on uranium adsorption performance (b)

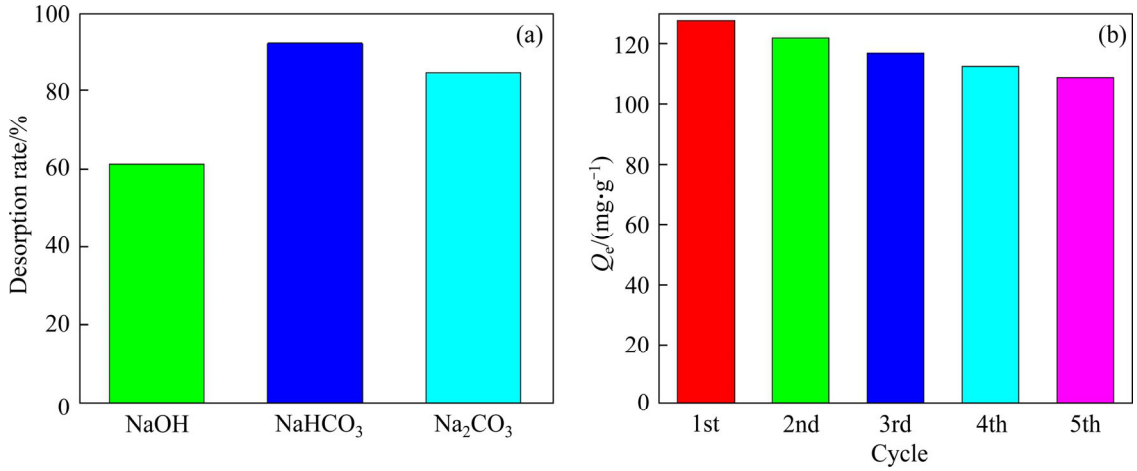

Figure 10 Desorption rate of different desorption agents (a), adsorption capacity for five cycles (b)

morphology of GO, rGO, $CoFe_2O_4$, and $CoFe_2O_4$@rGO were characterized by XRD, SEM, TEM, VSM, etc., and tested for uranium adsorption in aqueous media. The effects of pH, adsorption time and initial concentration of uranium on the adsorption behaviour of rGO, $CoFe_2O_4$, and $CoFe_2O_4$@rGO were investigated. The results show that $CoFe_2O_4$@rGO performs well for uranium adsorption, and pH has a significant effect on adsorption capacity. At a solution pH of 5, the uranium adsorption capacity of $CoFe_2O_4$@rGO is 127.6 mg/g, which is 1.31 and 2.43 times that of rGO and pure $CoFe_2O_4$, respectively. The uranium kinetic and adsorption isotherm data of $CoFe_2O_4$@rGO are more closely fitted to the quasi-second-order kinetic equation of Langmuir isotherm model. It is envisaged that the magnetic $CoFe_2O_4$@rGO composite is a promising material for the treatment of uranium-containing wastewater.

Contributors

The overarching research goals were developed by WU Shui-sheng and YI Bing. LAN Dong-hui and ZHANG Xiao-wen carried out mechanical tests. HUANG Yi and DENG Xing-hong analyzed the data. WU Shui-sheng and AU Chak-tong wrote the paper. All authors replied to reviewers' comments and revised the final version.

Conflict of interest

All authors declare that they have no conflict of interest.

References

[1] YANG Ai-li, YANG Peng, HUANG C P. Effect of Mg(II) on the removal of uranium from low radioactive wastewater by flocculation using polyacrylamide [J]. Journal of Hazardous, Toxic, and Radioactive Waste, 2017, 21(4): 04017006. DOI:

10.1061/(asce)hz.2153-5515.0000359.

[2] ZHANG C, DODGE C J, MALHOTRA S V, FRANCIS A J. Bioreduction and precipitation of uranium in ionic liquid aqueous solution by *Clostridium sp* [J]. Bioresource Technology, 2013, 136: 752−756. DOI: 10.1016/j.biortech.2013.03.085.

[3] SHEN Jun-jie, SCHÄFER A. Removal of fluoride and uranium by nanofiltration and reverse osmosis: A review [J]. Chemosphere, 2014, 117: 679−691. DOI: 10.1016/j.chemosphere.2014.09.090.

[4] SREENIVAS T, RAJAN K C. Studies on the separation of dissolved uranium from alkaline carbonate leach slurries by resin-in-pulp process [J]. Separation and Purification Technology, 2013, 112: 54−60. DOI: 10.1016/j.seppur.2013.03.050.

[5] LINGAMDINNE L P, CHOI Y L, KIM I S, YANG J K, KODURU J R, CHANG Y Y. Preparation and characterization of porous reduced graphene oxide based inverse spinel nickel ferrite nanocomposite for adsorption removal of radionuclides [J]. Journal of Hazardous Materials, 2017, 326: 145−156. DOI: 10.1016/j.jhazmat.2016.12.035.

[6] LI J, WANG X, ZHAO G, CHEN C, CHAI Z, ALSAEDI A, HAYAT T, WANG X. Metal-organic framework-based materials: Superior adsorbents for the capture of toxic and radioactive metal ions [J]. Chemical Society Reviews, 2018, 47(7): 2322−2356. DOI: 10.1039/c7cs00543a.

[7] TOBILKO V, SPASONOVA L, KOVALCHUK I, KORNILOVYCH B, KHOLODKO Y. Adsorption of uranium (VI) from aqueous solutions by amino-functionalized clay minerals [J]. Colloids and Interfaces, 2019, 3(1): 41. DOI: 10.3390/colloids3010041.

[8] ANIRUDHAN T S, JALAJAMONY S. Ethyl thiosemicarbazide intercalated organophilic calcined hydrotalcite as a potential sorbent for the removal of uranium(VI) and thorium(IV) ions from aqueous solutions [J]. Journal of Environmental Sciences, 2013, 25(4): 717−725. DOI: 10.1016/S1001-0742(12)60064-3.

[9] GU Peng-cheng, ZHANG Sai, LI Xing, WANG Xiang-xue, WEN Tao, JEHAN R, ALSAEDI A, HAYAT T, WANG Xiang-ke. Recent advances in layered double hydroxide-based nanomaterials for the removal of radionuclides from aqueous solution [J]. Environmental Pollution, 2018, 240: 493−505. DOI: 10.1016/j.envpol.2018.04.136.

[10] CHOUYYOK W, WARNER C L, MACKIE K E, WARNER M G, GILL G A, ADDLEMAN R S. Nanostructured metal oxide sorbents for the collection and recovery of uranium from seawater [J]. Industrial & Engineering Chemistry Research, 2016, 55(15): 4195−4207. DOI: 10.1021/acs.iecr.5b03650.

[11] WEN Zhen-qian, YAO Yi-xuan, NIU Yu-qing, ZHOU Gen-mao, XU Guo-long, ZHONG Hong. Adsorption mechanism of weakly basic anion exchange resin for uranium in acidic leaching solution containing uranium [J]. Journal of Central South University (Science and Technology), 2016, 47(6): 1867−1871. (in Chinese)

[12] ALI I, BASHEER A A, MBIANDA X Y, BURAKOV A, GALUNIN E, BURAKOVA I, MKRTCHYAN E, TKACHEV A, GRACHEV V. Graphene based adsorbents for remediation of noxious pollutants from wastewater [J]. Environment International, 2019, 127: 160−180. DOI: 10.1016/j.envint.2019.03.029.

[13] WU Zhong-shuai, WANG Da-wei, REN Wen-cai, ZHAO Jin-ping, ZHOU Guang-min, LI Feng, CHENG Hui-ming. Anchoring hydrous RuO_2 on graphene sheets for high-performance electrochemical capacitors [J]. Advanced Functional Materials, 2010, 20(20): 3595−3602. DOI: 10.1002/adfm.201001054.

[14] ZHAO Dong-lin, ZHU Hong-yu, WU Chang-nian, FENG Shao-jie, ALSAEDI A, HAYAT T, CHEN Chang-lun. Facile synthesis of magnetic Fe_3O_4/graphene composites for enhanced U(VI) sorption [J]. Applied Surface Science, 2018, 444: 691−698. DOI: 10.1016/j.apsusc.2018.03.121.

[15] BAI Song, SHEN Xiao-ping, ZHONG Xin, LIU Yang, ZHU Guo-xing, XU Xiang, CHEN Kang-min. One-pot solvothermal preparation of magnetic reduced graphene oxide-ferrite hybrids for organic dye removal [J]. Carbon, 2012, 50(6): 2337−2346. DOI: 10.1016/j.carbon.2012.01.057.

[16] CHEN Teng, DU Ping, JIANG Wei, LIU Jie, HAO Ga-zi, GAO Han, XIAO Lei, KE Xiang, ZHAO Feng-qi. A facile one-pot solvothermal synthesis of $CoFe_2O_4$/RGO and its excellent catalytic activity on thermal decomposition of ammonium perchlorate [J]. RSC Advances, 2016, 6(87): 83838−83847. DOI: 10.1039/c6ra16448j.

[17] ZHANG Kun, LI Jun-jian, WU Fan, SUN Meng-xiao, XIA Yi-lu, XIE A-ming. Sandwich $CoFe_2O_4$/RGO/$CoFe_2O_4$ nanostructures for high-performance electromagnetic absorption [J]. ACS Applied Nano Materials, 2019, 2(1): 315−324. DOI: 10.1021/acsanm.8b01927.

[18] ZHU Yan-fang, LV X, ZHANG Li-li, GUO Xiao-dong, LIU Dai-jun, CHEN Jian-jun, JI Jun-yi. Liquid-solid-solution assembly of $CoFe_2O_4$/graphene nanocomposite as a high-performance lithium-ion battery anode [J]. Electrochimica Acta, 2016, 215: 247−252. DOI: 10.1016/j.electacta.2016.08.057.

[19] SHARMA N, OJHA H, BHARADWAJ A, PATHAK D P, SHARMA R K. Preparation and catalytic applications of nanomaterials: A review [J]. RSC Advances, 2015, 5(66): 53381−53403. DOI: 10.1039/C5RA06778B.

[20] CORRADI A B, BONDIOLI F, FOCHER B, FERRARI A M, GRIPPO C, MARIANI E, VILLA C. Conventional and microwave-hydrothermal synthesis of TiO_2 nanopowders [J]. Journal of the American Ceramic Society, 2005, 88(9): 2639−2641. DOI: 10.1111/j.1551-2916.2005.00474.x.

[21] MA Jun, LIU Chang-hua, LI Rui, WANG Jia. Properties and structural characterization of oxide starch/chitosan/graphene oxide biodegradable nanocomposites [J]. Journal of Applied Polymer Science, 2012, 123(5): 2933−2944. DOI: 10.1002/app.34901.

[22] WEN Xiao-feng, DU Chun-yan, ZENG Guang-ming, HUANG Dan-lian, ZHANG Jin-fan, YIN Ling-shi, TAN Shi-yang, HUANG Lu, CHEN Hong. A novel biosorbent prepared by immobilized *Bacillus licheniformis* for lead removal from wastewater [J]. Chemosphere, 2018, 200: 173−179. DOI: 10.1016/j.chemosphere.2018.02.078.

[23] LIU Wen, ZHAO Xiao, WANG Ting, ZHAO Dong-ye, NI Jin-ren. Adsorption of U(VI) by multilayer titanate nanotubes: Effects of inorganic cations, carbonate and natural organic matter [J]. Chemical Engineering Journal, 2016, 286: 427−435. DOI: 10.1016/j.cej.2015.10.094.

[24] FATHY M, GOMAA A, TAHER F A, EL-FASS M M, KASHYOUT A E H B. Optimizing the preparation parameters of GO and rGO for large-scale production [J]. Journal of Materials Science, 2016, 51(12): 5664−5675. DOI: 10.1007/s10853-016-9869-8.

[25] GABAL M A, AL-JUAID A A, EL-RASHED S, HUSSEIN M A. Synthesis and characterization of nano-sized $CoFe_2O_4$ via facile methods: A comparative study [J]. Materials Research Bulletin, 2017, 89: 68−78. DOI: 10.1016/j.materresbull.2016.12.048.

[26] MERMOUX M, CHABRE Y, ROUSSEAU A. FTIR and ^{13}C NMR study of graphite oxide [J]. Carbon, 1991, 29(3): 469−474. DOI: 10.1016/0008-6223(91)90216-6.

[27] CHEN Shui-ping, HONG Jian-xun, YANG Hong-xiao, YANG Ji-zhen. Adsorption of uranium (VI) from aqueous solution using a novel graphene oxide-activated carbon felt composite [J]. Journal of Environmental Radioactivity, 2013, 126: 253−258. DOI: 10.1016/j.jenvrad.2013.09.002.

[28] SUN Yu-bing, DING Cong-cong, CHENG Wen-cai, WANG Xiang-ke. Simultaneous adsorption and reduction of U(VI) on reduced graphene oxide-supported nanoscale zerovalent iron [J]. Journal of Hazardous Materials, 2014, 280: 399−408. DOI: 10.1016/j.jhazmat.2014.08.023.

[29] YIN Wen-zhu, HAO Shuo, CAO Hua-qiang. Solvothermal synthesis of magnetic $CoFe_2O_4$/rGO nanocomposites for highly efficient dye removal in wastewater [J]. RSC Advances, 2017, 7(7): 4062−4069. DOI: 10.1039/C6RA26948F.

[30] SUN Yu-bing, YANG Shi-tong, SHENG Guo-dong, GUO Zhi-qiang, WANG Xiang-ke. The removal of U(VI) from aqueous solution by oxidized multiwalled carbon nanotubes [J]. Journal of Environmental Radioactivity, 2012, 105: 40−47. DOI: 10.1016/j.jenvrad.2011.10.009.

(Edited by HE Yun-bin)

中文导读

$CoFe_2O_4$@rGO 纳米复合材料的微波水热合成、表征及其吸附性能

摘要：通过微波水热法合成磁性 $CoFe_2O_4$@rGO 纳米复合材料。XRD、Raman、TEM/HRTEM、FTIR、BET 和 VSM 表征结果表明，尺寸约为 13 nm 的尖晶石型 $CoFe_2O_4$ 纳米粒子分散锚定在石墨烯片上，其饱和磁化强度为 46.7 mA/(m^2·g)，满足磁分离要求。研究了不同 pH 值、初始浓度等条件对 $CoFe_2O_4$@rGO 铀吸附容量的影响，确定了铀在水中的吸附行为并拟合了吸附动力学方程。结果表明在 pH=5 时，$CoFe_2O_4$@rGO 纳米复合材料吸附铀的能力为 127.6 mg/g，分别是 rGO 和纯 $CoFe_2O_4$ 的 1.31 和 2.43 倍。吸附过程符合 Langmuir 和准二级动力学模型。$CoFe_2O_4$@rGO 纳米复合材料优良的吸附性能使其在处理铀污染水方面具有潜在的用途。

关键词：$CoFe_2O_4$；石墨烯；铀；吸附性能